CHAPTER 5

GEOCHEMISTRY

Data sets for the whole rock major, minor, trace and rare earth element (REE) geochemistry of selected samples of biotite schist, graphite schist, Mn- carbonate schist, Mn-calcite marble as well as rhodochrosite marble are presented. Elemental concentrations correlate well with the mineralogic and petrographic observations outlined in previous chapters. Thirty samples comprising all the lithologies were selected for analysis and submitted to ACME Analytical Labs ltd. (Canada). Major element data were acquired using *X-ray fluorescence spectrometry* (XRF) on fused beads and pressed pellets. Trace element data, including rare earth-elements (REE) were obtained using *Inductively Coupled Plasma Mass Spectrometry* (ICP-MS). Stable isotope geochemistry data for the carbonate species are also presented and discussed. Stable isotope analysis was performed on selected carbonate bearing samples from the three drill cores using an automated *Mass Spectrometer* at the Council of Geosciences, Pretoria (Dr. U. Horstmann).

5.1 Results

5.1.1 Major Element Geochemistry

Petrographic studies identified five lithologies: biotite schist, graphite schist, Mn-carbonate schist, Mn-calcite marble and rhodochrosite marble. The major element geochemistry, however, shows two extremes in composition, the one dominated by alumina and silica while the other is carbonate-rich. Based on the major element composition, the lithologies were therefore subdivided into two fundamental groups. The one group encompasses biotite schist and graphite schist, the other group is constituted by Mn-carbonate schist, Mn-calcite marble and rhodochrosite marble. The former is herein referred to as alumo-silicate rocks while the latter group is called carbonate-rich rocks.

5.1.1.1 Alumo – Silicate rocks

Whole rock chemical data for alumo-silicate rocks are presented in Table 5.1. There is no clear geochemical distinction between graphite schist and biotite schist (Fig 5.1). They are marked by high concentrations of SiO_2 (45 – 79wt. %), Al_2O_3 (mostly above 5 wt.%) and TiO_2 (0.5 – 1 wt. %). Total Fe varies between 3 – 12 wt. %. Most notable are the extremely low and erratic concentrations of MnO in both petrological groups ranging from 0.01 – 4.4 wt.%. The concentration of MnO appears to be inversely related to the concentration of SiO_2. The Mn/Fe ratio is always less than 1. Concentrations of CaO and MgO are low and rather consistent, on average < 5 wt. %. With the exception of these two elements all the others display an antipathetic relationship with SiO_2 (Fig.5.1). The oxides of Na and K display variable but relatively high concentrations ranging from 0.1 – 4 wt.% and 0.3 – 3wt.%, respectively. Phosphorous is somewhat consistent at ~ < 0.1 wt. %. The LOI is very variable, between 1 – 13 wt.%.

5.1.1.2 Mn-carbonate rocks

Major element data of selected samples are shown in Table 5.2. MnO predominates in all the three petrological groups followed by CO_2 (expressed as LOI), SiO_2, Fe_2O_3, CaO, MgO and Al_2O_3. On average, rhodochrosite marble is most enriched in MnO, CO_2 and CaO, followed by Mn-calcite marble and Mn-carbonate schist. The MnO content varies between 46 – 54 wt. % in rhodochrosite marble, 36 – 60wt.% in Mn-calcite marble and 19 – 43wt.% in Mn-carbonate schist. The Fe content is rather consistent and similar to the alumo-silicate rocks. Mn/Fe ratios are always > 1, but are highest in rhodochrosite marble, up to 56.4. The rocks are characterized by variable contents of SiO_2 that are, on average, drastically lower than in the alumo-silicate group. The SiO_2 content is lowest and variable in rhodochrosite marble (1.2 – 10 wt.%), higher and consistent in Mn-calcite marble (22 – 26 wt%) and highest in Mn-carbonate schists (36 – 42 wt.%).

Table 5.1: Major element geochemistry of alumo-silicate rocks from the Serra do Navio deposit. NB: All data in wt. %.

Rock type	**Graphite schist**			**Biotite schist**					
SAMPLE	**DH114-J**	**DH116-K**	**DH116-P**	**D114-O**	**D114-P**	**D116-N**	**D116-Q**	**D116-T**	**DH140-K**
SiO_2	62.7	48.5	57.3	49.6	68.5	66.7	78.7	61.7	43.9
TiO_2	0.8	0.83	0.63	0.74	0.88	0.83	0.36	0.76	1.14
Al_2O_3	14.3	12.5	12.3	13.6	9.57	14.2	4.64	15.3	17.9
Fe_2O_3 (T)	4.40	16.0	10.9	11.7	8.49	2.59	9.01	11.2	8.84
MnO	0.55	4.37	1.38	2.44	0.12	0.48	0.15	0.08	3.17
MgO	1.12	1.92	0.67	2.45	3.61	1.64	3.23	2.43	4.53
CaO	2.44	1.16	2.09	1.39	4.23	3.68	2.47	0.65	1.28
Na_2O	3.94	3.71	2.49	3.55	0.10	2.30	0.21	0.06	3.81
K_2O	2.16	4.33	0.76	0.93	0.71	5.45	0.28	2.77	1.48
P_2O_5	0.14	0.11	0.06	0.11	0.06	0.04	0.07	0.14	0.07
LOI	6.1	5.5	12.2	13.3	2.0	1.8	1.0	4.8	13.2
Mn/Fe	0.13	0.27	0.13	0.21	0.01	0.19	0.02	0.01	0.36
TOTAL	98.7	99	100.8	99.8	99.3	99.7	100.2	100	99.3

Data supplied by ACME Analytical Laboratories ltd. (Canada) Fe_2O_3 (T) = Total Fe (expressed as Fe_2O_3)

Table 5.2: Major element geochemistry of carbonate rocks from the Serra do Navio deposit. NB: All data in wt. %.

Rock type	**Rhodochrosite marble**							
SAMPLE	**DH114-B**	**DH114-L**	**DH116-E**	**DH116-I**	**DH116-M**	**DH140-L**	**DH140-M**	**DH140-N**
SiO_2	5.12	8.68	1.52	2.15	2.84	7.71	6.31	10.9
TiO_2	0.2	0.09	0.04	0.07	0.15	0.41	0.17	0.13
Al_2O_3	1.98	1.76	1.36	2.07	2.78	5.09	2.11	2.22
Fe_2O_3 (T)	6.06	1.27	3.78	1.62	0.94	2.40	1.91	1.55
MnO	50.3	53.4	45.9	54.1	53	51.7	51.7	46.5
MgO	3.49	3.26	4.97	3.67	2.4	3.75	4.73	5.77
CaO	5.66	5.33	9.58	4.39	6.15	3.85	6.59	10.6
Na_2O	0.03	0.03	< .01	< .01	0.02	0.03	0.02	0.05
K_2O	0.05	0.04	0.10	0.04	0.03	0.05	0.15	0.40
P_2O_5	0.18	< .01	0.05	0.01	< .01	0.05	< .01	0.04
LOI	26.2	24.9	31.6	30.8	30.3	24.6	25.3	20.1
Mn/Fe	8.3	42.1	12.1	33.4	56.4	21.5	27.0	30.0
TOTAL	99.3	98.9	98.9	98.9	98.8	99.7	99.0	98.5

Data supplied by ACME Analytical Laboratories ltd. (Canada) Fe_2O_3 (T) = Total Fe (expressed as Fe_2O_3)

Table 5.2 contd.

Rock type	Mn-carbonate schist						Mn-calcite marble					
SAMPLE	DH114-A	DH116-A	DH116-B	DH140-A	DH140-C	DH140-D	DH114-K	DH114-C	DH114-E	DH116-H	D116-J	DH140-O
SiO_2	36.4	40.5	41.9	40.4	39.0	39.9	22.0	26.2	23.1	24.2	24.9	22.4
TiO_2	0.22	0.43	0.08	0.07	0.10	0.18	0.26	0.27	0.19	0.04	0.22	0.09
Al_2O_3	4.24	8.53	2.51	0.92	3.67	2.22	4.16	3.28	3.29	1.44	3.48	1.87
Fe_2O_3 (T)	6.19	5.90	8.64	5.04	3.84	5.46	1.94	11.2	4.19	2.34	6.71	5.71
MnO	43.0	33.9	19.7	42.6	42.3	39.8	50.5	36.5	50.2	60.2	47.4	52.4
MgO	3.87	3.97	6.84	2.27	2.56	3.01	5.5	8.5	6.03	3.20	6.18	5.24
CaO	3.99	3.65	9.22	3.45	2.64	3.72	4.93	8.23	4.74	3.65	4.66	5.78
Na_2O	0.03	0.01	0.04	0.01	< .01	< .01	0.03	< .01	0.02	0.01	0.03	0.01
K_2O	0.04	< .02	< .02	0.02	< .02	< .02	0.42	0.60	0.39	< .02	0.14	< .02
P_2O_5	< .01	0.11	0.05	< .01	0.01	0.27	< .01	0.17	< .01	< .01	0.05	< .01
LOI	1.2	3.2	10.6	4.4	5.0	4.8	9.5	4.4	7.0	3.6	5.4	5.1
Mn/Fe	7.0	5.7	2.3	8.4	11.0	7.3	26	3.2	12.0	25.7	7.1	9.2
TOTAL	99.5	100.1	99.7	99.2	99.1	99.3	99.3	99.3	99.1	98.7	99.2	98.6

Data supplied by ACME Analytical Laboratories ltd. (Canada) Fe_2O_3 (T) = Total Fe (expressed as Fe_2O_3)

The contents of Ca and Mg are particularly consistent in the carbonate group of rocks and notably higher than in the alumo-silicate rock (3 – 8 wt.% CaO and 2 – 8 wt.% MgO, respectively). The TiO_2 content is very low with an average < 0.1 wt.%; Na_2O and K_2O are similarly low and very rarely exceed 0.01 wt.%. Phosphorous concentrations are moderate (0.1 wt.%) to very low (<0.01 wt.)

The three petrological groups within the carbonate lithologies are geochemically distinct in their major element composition. On binary plots (Fig.5.2), the three groups all plot in consistently different fields. These fields seem to be controlled by the amount of Si relative to Mn in these rocks. Minor elements (Ti, Al, Fe, Mg and Ca) all appear to be positively correlated with SiO_2 for the all three petrological groups. MnO, however, is negatively correlated with SiO_2, a feature reflected by all three (Fig. 5.2d) lithologic groups. This correlation may be due to closure effect. On a ternary plot, the carbonate-rich rocks plot well removed from the alumo-silicate rocks (Fig. 5.3).

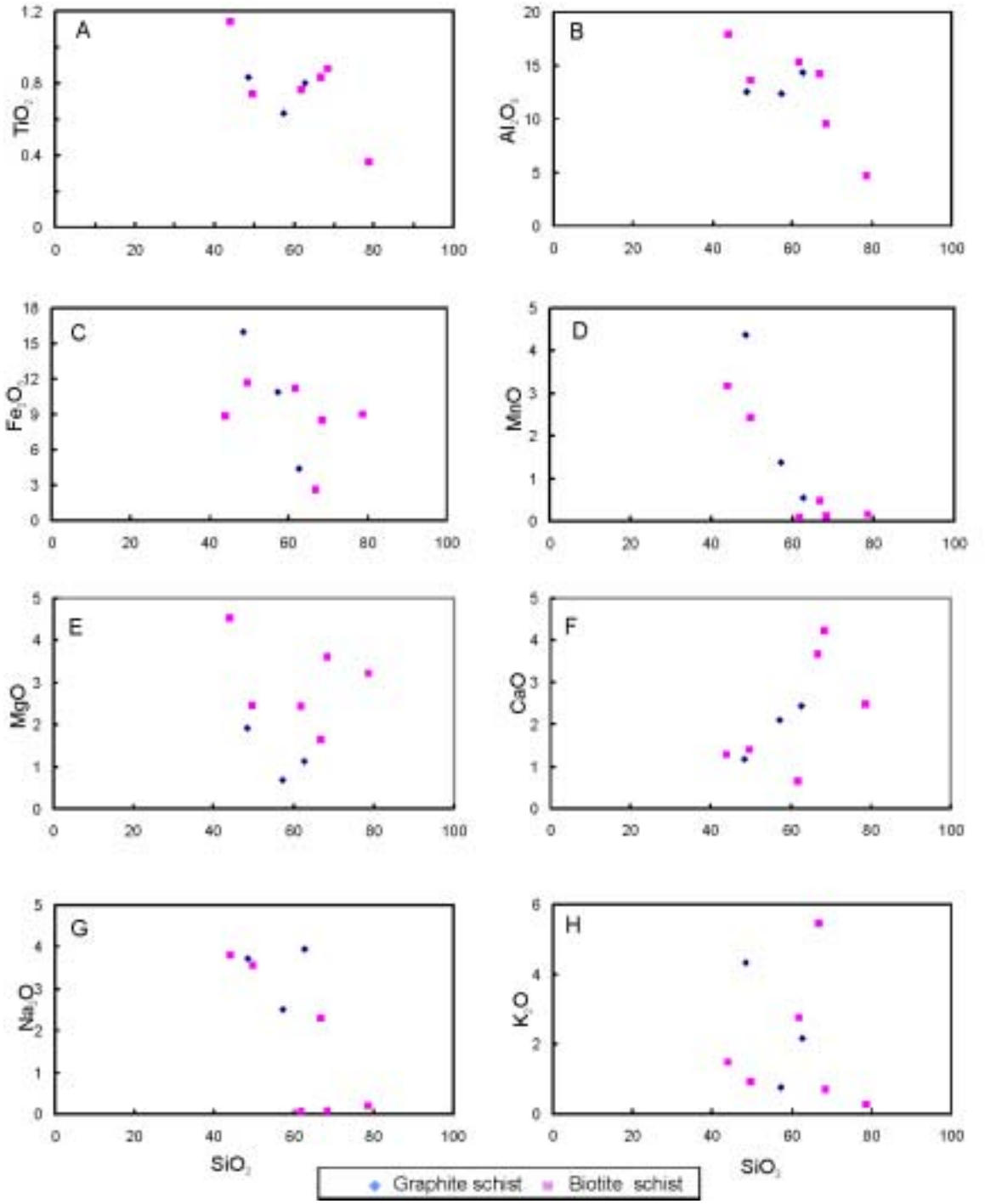

Fig.5.1: Binary plots (wt.%) illustrating the major element geochemistry of the alumo-silicate group of rocks from the Serra do Navio deposit. Note the complete overlap of major element geochemistry of both lithologies and negative correlation of SiO_2 with all other major elements with the exception of MgO and CaO.

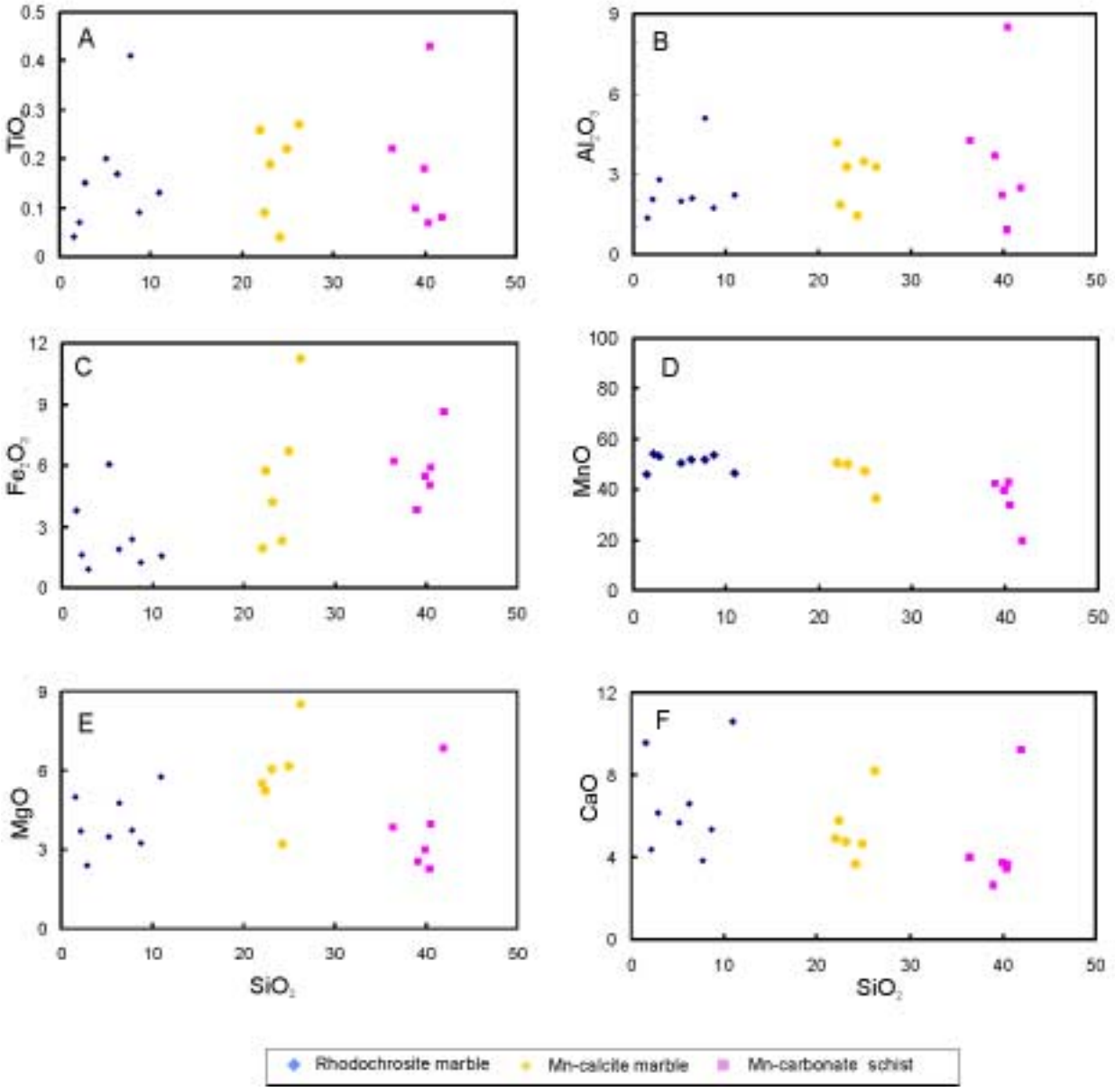

Fig.5.2: Binary plots (wt.%) illustrating the major element geochemistry of the Mn-carbonate-rich group of rocks from the Serra do Navio deposit. The three petrologically distinct lithologies consistently plot in particular fields.

But even within the carbonate-rich group, the three petrologic types are well distinguished from one another. An interesting feature observed in these plots is that the major element geochemistry of these three lithologies is not a function of Al, Ca or Mg

concentration, but a function of SiO_2 concentration (Fig. 5.3). The relative abundance of SiO_2 appears to determine the lithological group to which each sample belongs.

Compared to the alumo-silicate rocks, the carbonate rocks are depleted in SiO_2, Al_2O_3 and Fe_2O_3 (Fig.5.3). MgO concentrations are rather similar while MnO and CaO are markedly enriched. The alumo-silicates are further characterized by high concentrations of Na_2O and K_2O as compared to carbonate rich rocks.

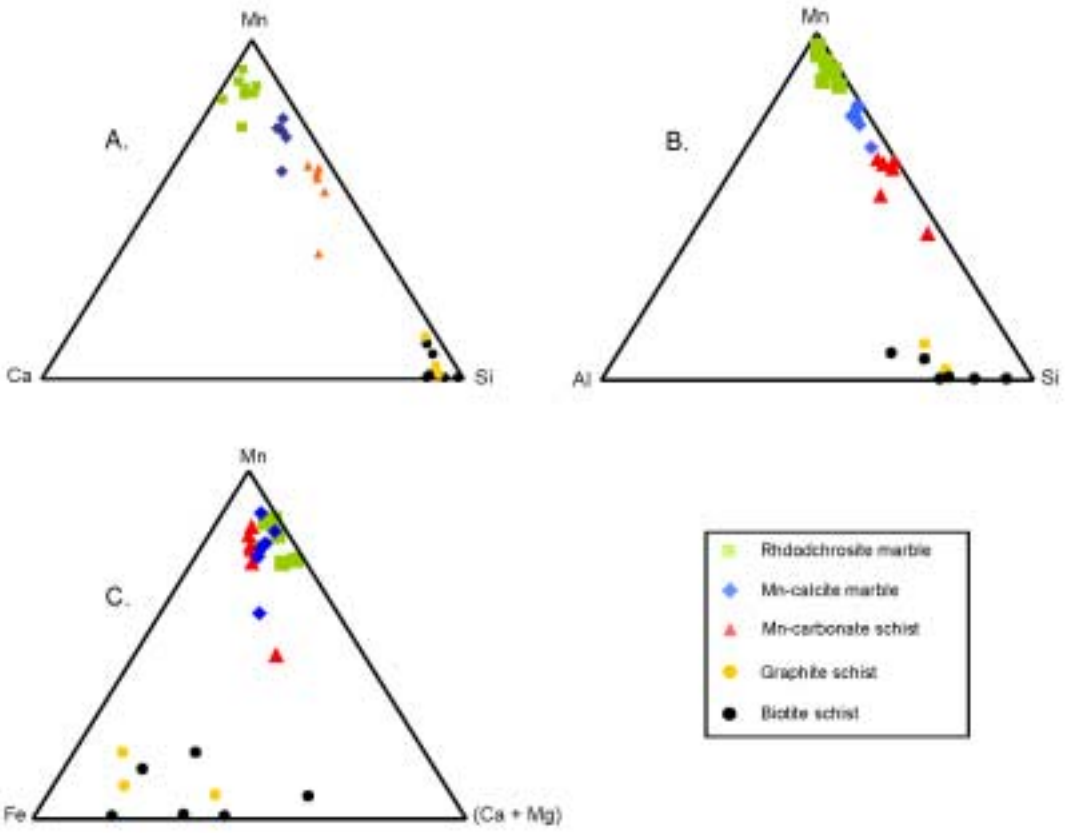

Fig.5.3: Ternary plots (wt. %) contrasting the major element geochemistry of the alumo-silicate and carbonate-rich groups of lithologies. A: Mn-Si-Ca; The three petrologically distinct carbonate-rich lithologies plot in well-defined non-overlapping fields. The biotite schist and graphite schist data in contrast occupy the same field, but are well removed from the carbonate-rich lithologies. B: Mn-Si-Al; The difference between the carbonate-rich lithologies is clearly due to negative covariation between Mn and Si. Note Mn-poor but Al-enriched composition of biotite schist and graphite schist. C: Mn-(Ca + Mg)-Fe. The three corners represent carbonate constituents. The three carbonate-rich lithologies overlap whereas the alumo-silicates scatter widely.

5.1.2 Trace element geochemistry

The presentation of trace element data is based on the subdivision of rock types into alumo-silicate rocks and carbonate-rich lithologies. This is because, just like in the major element compositions, there is a coherent distribution of trace elements in both the alumo-silicates and the carbonate-rich rocks.

5.1.2.1. Alumo-silicate rocks

Both biotite schist and graphite schist show a remarkable similarity in trace element geochemistry. Even though they are petrographically different, most trace element concentrations, including Th, U, Rb, Z, Y, NB, V and base metals are rather similar in the two rock types (Table 5.3).

In a plot on the Upper Continental Crust (UCC) spider diagram of Taylor and McLennan (1981) the trace elements in the alumo-silicate rocks from the Serra do Navio deposit show rather flat distribution patterns (Fig. 5.4). Most trace element concentrations show a uniform distribution and a range of concentration corresponding closely to UCC. Both biotite schist and graphite schist are, however, depleted in K, P and Sr with respect to UCC whereas Ba and Rb are both highly elevated relative to upper crustal abundances, though Ba shows a wider variation (81 – 4000ppm) than Rb (12 – 176ppm).

Rb varies positively with K_2O (Fig. 5.5a). Ba is weakly correlated with K and MnO but strongly varies positively with Al_2O_3 (Fig. 5.5b, c and d). The concentrations of Th, U and V are uniform in all the samples from both petrologic groups. There is a large variability in V but no correlation with MnO (Fig. 5.5e). Zr and Y display coherent elevated concentrations with Zr rarely below 100ppm. Strong positive correlation exists between Zr and TiO_2 (Fig. 5.5h). Sr is somewhat uniform in both petrologic groups, and strongly covaries with CaO. Sc concentrations are similarly uniform in both lithological groups (~ 16ppm) and are positively correlated with TiO_2. Base metals, especially Co, show a uniform distribution with concentrations above 100ppm. Ni concentrations strongly co-vary with Co and MnO content in both alumo-silicate rocks (Fig. 5.5f). Co

concentration is on average higher in graphite schist (~ 145ppm) compared to biotite schist (~ 48ppm). Pb is less abundant with a range of 8 – 70ppm in biotite schist and 16 – 95ppm in graphite schist. The concentrations of Pb and Zn are positively related to Co and V. The unusual great variability of Cu (25 – 2355ppm) is noteworthy and may represent covariation of Cu with a major element, in particular Fe since a strong positive correlation of Cu with Fe_2O_3 is observed.

Table 5.3: Trace element geochemistry of alumo-silicate rocks at the Serra do Navio deposit. All data in ppm.

Rock type	**Graphite schist**			**Biotite schist**					
Sample	**DH114-J**	**DH116-K**	**DH116-P**	**DH114-O**	**DH114-P**	**DH116-N**	**DH116-Q**	**DH116-T**	**DH140-K**
Sc	10	23	17	20	14	13	8	19	23
V	137	149	127	138	97	141	95	184	139
Cr	151	192	431	130	157	397	486	335	246
Co	132	186	123	150	97	35	25	24	31
Ni	144	708	466	522	71	135	48	96	261
Cu	246	2355	311	604	65	27	65	54	26
Zn	82	176	74	159	90	139	19	135	135
Rb	98	167	33	37	79	122	12	117	49
Sr	258	211	162	192	98	249	138	29	293
Y	27	39	46	46	24	28	14	32	33
Zr	100	95	70	115	288	133	107	111	148
Nb	9	8	7	9	10	10	4	10	17
Ba	4863	4133	251	600	273	764	82	344	3115
Pb	16	50	95	70	18	11	8	29	14
Th	10	7	6	12	9	13	5	11	16
U	3	4	3	4	4	4	2	4	4

Data supplied by ACME Analytical Laboratories ltd. (Canada)

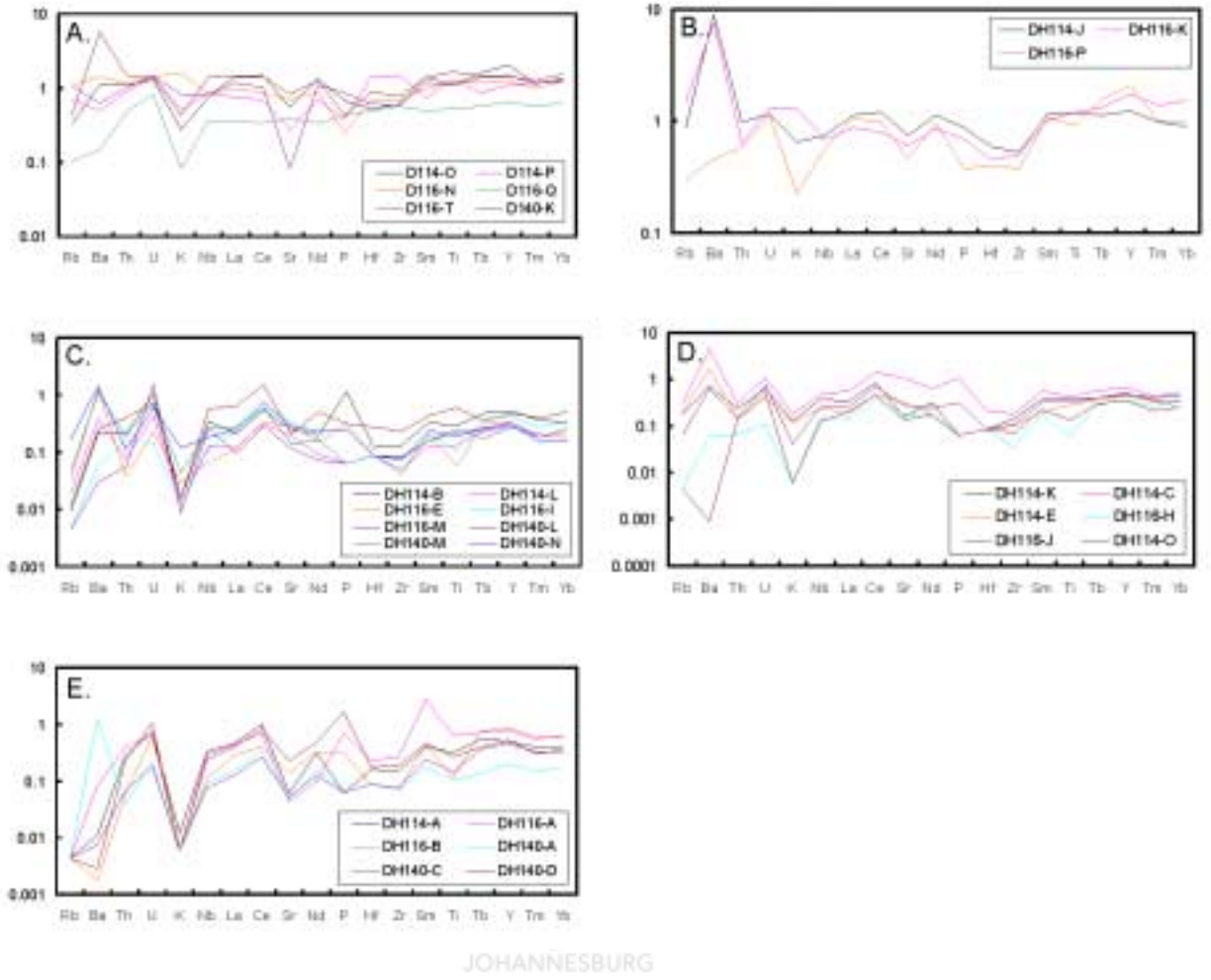

Fig. 5.4: Spider diagram of Upper Continental Crust (UCC) - normalized trace element concentrations of different lithological groups of the Serra do Navio deposit. UCC = 1. A: Biotite schist. Most elements plot close to upper continental crustal estimates; B: Graphite schist. Very similar to biotite schist with most trace elements ~1 except for a marked enrichment in Ba; C: Rhodochrosite marble; D: Mn-calcite marble; E: Mn-carbonate schist. All carbonate rich rocks are depleted in most trace element concentrations with respect to UCC (Taylor and McLennan, 1981).

5.1.1.2 Carbonate rocks

The trace element geochemistry of selected samples from this group is reported in Table 5.4. A fairly consistent pattern in trace element concentration is common across all the samples.

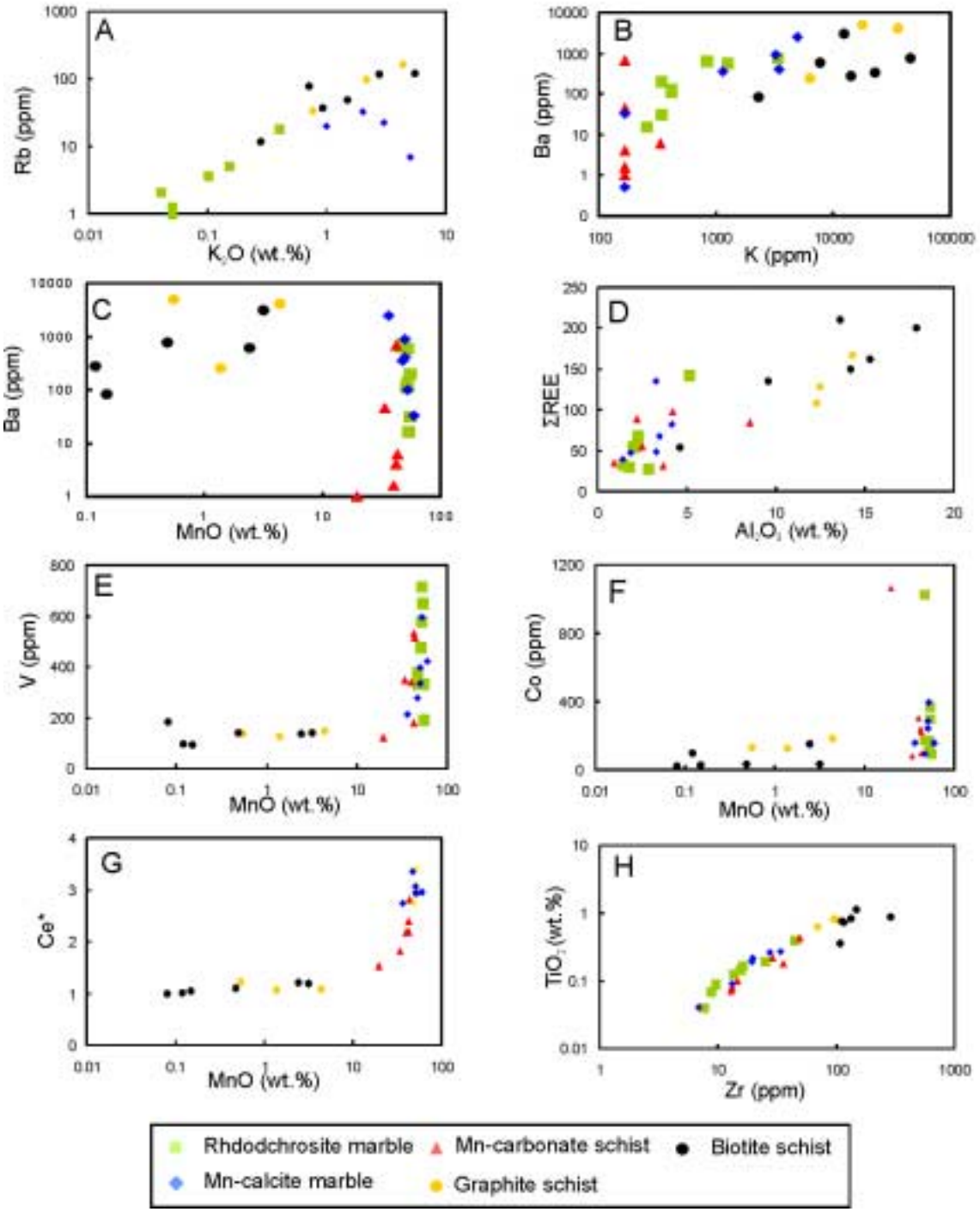

Fig.5.5: Binary plots of trace elements of the different lithological groups of the Serra do Navio deposit. A: K_2O vs. Rb; B: K vs. Ba; C: MnO vs. Ba; D: Al_2O_3 vs. ∑REE; E: V vs. MnO; F: Co vs. MnO; G: MnO vs. Ce*; H: TiO_2 vs. Zr.

Table 5.4: Trace element geochemistry of carbonate rocks at the Serra do Navio deposit. All data in ppm

Rock type	**Rhodochrosite marble**							
Sample	**DH114-B**	**DH114-L**	**D116-E**	**DH116-I**	**DH116-M**	**DH140-L**	**DH140-M**	**DH140-N**
Sc	5	4	2	3	3	8	3	3
V	478	335	379	194	652	718	581	334
Cr	62	34	21	41	89	198	62	75
Co	141	305	181	97	372	174	162	1030
Ni	388	766	502	337	907	643	609	1824
Cu	18	3	39	2	5	9	448	438
Zn	153	114	134	2	87	297	728	963
Rb	1	2	4	0	0	1	5	19
Sr	87	67	103	121	41	75	49	102
Y	12	6	7	9	7	10	6	7
Zr	25	10	8	9	15	44	16	14
Nb	4	2	1	1	3	7	3	2
Ba	118	214	688	33	17	137	600	790
Pb	74	7	11	6	3	41	24	69
Th	2	1	0	2	1	4	2	1
U	3	1	1	0	4	2	2	2

Data supplied by ACME Analytical Laboratories ltd. (Canada)

In a UCC spider diagram (Taylor and McLennan, 1981) most trace element compositions of the carbonate-rich lithologies are below upper crustal values (Fig. 5.4 c – e). Ba, U, P, Ce and Sm are, on average, all only moderately enriched while K, Ti and Zr are depleted especially in rhodochrosite and Mn-calcite marble, compared to alumo-silicates. The scenario is somewhat similar in Mn-carbonate schist but for the great variability in Ba and P. Rb concentrations are low in both rhodochrosite marble and Mn-calcite (average ~ 10ppm) and much lower in Mn-carbonate schist (< 0.05ppm).

Table 5.4: contd. All data in ppm

Rock type	Mn-carbonate schist						Mn-calcite marble					
Sample	D114-A	DH116-A	DH116-B	D140-A	D140-C	D140-D	D114-K	DH114-C	DH114-E	DH116-H	D116-J	DH140-O
Sc	7	8	9	3	7	5	7	10	6	2	7	5
V	517	349	124	179	532	339	397	211	336	422	276	594
Cr	55	198	116	55	82	89	48	41	82	68	68	75
Co	97	82	1065	220	239	301	243	157	288	159	91	397
Ni	144	202	525	486	528	619	662	460	829	261	326	1078
Cu	21	4	48	24	72	10	7	10	4	13	23	12
Zn	208	88	151	176	71	109	313	691	327	274	361	541
Rb	0	0	0	0	0	0	20	33	23	0	7	0
Sr	21	15	49	17	18	82	56	372	111	62	100	47
Y	11	17	19	4	10	12	11	15	10	8	11	8
Zr	29	49	13	13	15	36	28	34	19	7	20	13
Nb	4	4	1	1	1	3	4	6	3	2	3	2
Ba	6	45	1	688	4	2	396	2497	901	33	355	98
Pb	11	3	3	11	18	13	4	33	21	11	4	12
Th	3	4	1	0	1	2	3	3	2	1	2	1
U	2	2	2	1	1	3	2	3	1	0	2	1

Data supplied by ACME Analytical Laboratories ltd. (Canada)

In rhodochrosite marble and Mn-calcite marble Rb covaries positively with K_2O (Fig. 5.5a). Ba concentrations (~ 500ppm average) for the three lithological groups are slightly lower than for the alumo-silicates. The correlation of Ba with MnO is significant and positive, but weakly positive with K and weakly negative with Al_2O_3 (Fig. 5.5 b and c). Concentrations of Sc (3 – 10ppm) and Cr (average 60ppm) are rather consistent within the carbonate rich rocks. Sc has a strong positive correlation with TiO_2 and Zr (Fig.5.5h). Sr concentrations are highest in Mn-calcite marble (56 – 372ppm) followed by rhodochrosite marble (41 –103ppm) and Mn-carbonate schist (15 – 80ppm). The correlation of Sr with CaO is weakly positive.

Compared to the alumo-silicate rocks, Th (1 – 4ppm,), U (1 – 3ppm and Nb (1 – 7ppm) are depleted in all three lithological groups, though their distribution is uniform. Concentrations of V, Ni, Co and Zn are all very high compared to the alumo-silicates and usually above 100ppm in the three petrological groups. Zn, V, Co and Ni all strongly covary with MnO (Fig. 5.5f). At least two samples of rhodochrosite marble (DH140-M and DH140-N) display high values of Co, Ni, Cu and Zn. Cu and Pb contents are variable in all three lithological groups, on average, but lower than in the alumo-silicates. A weak positive correlation of Cu and Pb with Fe_2O_3 exists.

Systematic differences between the alumo-silicate rocks and the carbonate rich lithologies include elevated concentrations of V, Ce and P and depleted concentrations of Th, U, Zr, Sc and Rb in the latter. Both groups are enriched in Ba relative to UCC, but the alumo-silicate group shows on average, greater concentrations and less variability. Depletion in K and Sr relative to UCC is noted in both groups but is conspicuous and much more variable in the carbonate rich rocks. In addition, most elements in the alumo-silicate group plot near the UCC whereas those of the carbonate rich group plot below the UCC (Fig.5.4).

5.1.3 Rare Earth Element Geochemistry

The rare earth elements (REE) belong to a coherent group of elements characterized by a similar ionic radius and trivalent oxidation state in most physiochemical environments in the earth's crust (Bau, 1991). However, various fractionation processes are known to have an effect on the distribution of REE in natural systems and usually become apparent as anomalies or enrichment/depletion trends in REE patterns that are normalized against well-known standards such as chondrite or average shale compositions (Rollinson, 1993). In this study all REE data are normalized against the Post Archean Average Shale (PAAS) of Taylor and McLennan (1985).

REE analyses have been obtained from selected samples of both alumo-silicate rocks and carbonate rocks. Analytical results of the aforementioned selected samples are given in

Tables 5.5 and 5.6. The graphical representation of the resultant PAAS normalized patterns is given in Fig. 5.6. The formulae for calculating the Ce* and Eu* anomalies are explained in the appendix.

Table 5.5: Rare earth element concentration of selected samples of alumo-silicate rocks from the Serra do Navio deposit. All data in ppm.

Rock type	**Graphite Schist**			**Biotite Schist**					
Sample	**DH114-J**	**DH116-K**	**DH116-P**	**DH114-O**	**DH114-P**	**DH116-N**	**DH116-Q**	**DH116-T**	**DH140-K**
La	33.9	26.2	31.4	43.6	22.5	29.9	11.0	35.7	42.2
Ce	77.1	50.5	62.5	95.8	44.6	55.1	21.6	65.1	92.3
Pr	6.7	4.8	5.9	8.3	4.6	5.7	2.3	6.9	8.2
Nd	29.1	22.0	25.0	34.8	18.3	23.4	8.8	28.4	32.2
Sm	5.2	4.5	4.8	6.2	3.4	4.5	2.2	5.3	6.2
Eu	1.1	0.8	2.0	1.4	0.8	1.0	0.2	1.3	1.5
Gd	4.5	4.6	5.0	6.3	3.3	4.2	2.0	5.3	5.1
Tb	0.7	0.8	1.0	1.0	0.6	0.8	0.4	0.9	0.9
Dy	3.6	5.4	5.3	5.9	3.3	4.1	1.9	4.8	4.8
Ho	0.7	1.0	1.0	1.1	0.7	0.8	0.4	1.0	1.0
Er	2.2	3.0	2.8	3.1	2.2	2.3	1.2	2.7	2.7
Tm	0.3	0.5	0.3	0.4	0.4	0.3	0.2	0.4	0.4
Yb	2.0	3.3	2.2	2.8	2.8	2.6	1.4	3.4	3.0
Lu	0.2	0.5	0.3	0.4	0.3	0.3	0.2	0.4	0.4
ΣREE	167.2	128.0	149.5	211.1	107.8	135.0	53.8	161.6	201.0
LREE/ HREE	10.8	5.6	7.2	9.0	6.8	7.7	5.9	7.5	9.9
Ce/Ce* (N)	1.2	1.0	1.1	1.2	1.0	1.0	1.0	1.0	1.1
Eu/Eu* (N)	1.1	0.8	1.9	1.0	1.1	1.1	0.5	1.2	1.3

Data supplied by ACME Analytical Laboratories ltd. (Canada)

5.1.3.1 Alumo-silicate rocks

REE plots for all samples of the alumo-silicate group display a relatively flat and uniform distribution pattern (Fig. 5.6a) with concentrations very similar to PAAS, i.e., the REE distribution observed in biotite schist and graphite schist corresponds closely to that of Post-Archean average shale. The REE distribution of all samples is similar and

characterized by mild enrichment of the Middle Rare Earth Elements (MREE) over the Light Rare Earth Elements (LREE) and Heavy Rare Earth Elements (HREE). The ΣREE lies in the range 50 – 200ppm. There is a strong positive correlation between ΣREE and Al_2O_3 (Fig. 5.5d). Some samples display a weak positive Ce anomaly but no Eu anomalies. There is no apparent correlation of the Ce anomaly with MnO (Fig.5.5g). This feature is common to both biotite schist and graphite schist.

Table 5.6: Rare element geochemistry of selected samples of carbonate rocks from the Serra do Navio deposit. All data in ppm.

Rock type	**Rhodochrosite marble**							
Sample	**DH114-B**	**DH114-L**	**DH116-E**	**DH116-I**	**DH116-M**	**DH140-L**	**DH140-M**	**DH140-N**
La	6.3	3.6	3.5	6.8	2.8	18.7	8.3	7.4
Ce	34.7	20.1	20.9	37.8	18.4	99.0	38.7	49.1
Pr	1.5	0.7	0.9	1.3	0.6	3.6	1.2	1.6
Nd	5.2	2.4	3.9	4.4	1.9	12.9	4.3	6.0
Sm	1.5	0.6	0.9	1.0	0.7	2.0	0.7	1.1
Eu	0.4	0.2	0.3	0.3	0.3	0.5	0.2	0.4
Gd	1.6	0.7	0.9	1.1	1.2	1.7	0.6	1.0
Tb	0.3	0.2	0.2	0.3	0.2	0.2	0.1	0.2
Dy	1.4	0.7	1.0	1.2	0.9	1.7	0.7	1.0
Ho	0.3	0.2	0.2	0.2	0.1	0.3	0.1	0.2
Er	0.9	0.6	0.7	0.7	0.5	0.8	0.5	0.5
Tm	0.1	0.1	0.1	0.1	0.1	0.1	0.1	0.1
Yb	0.7	0.4	0.5	0.8	0.6	1.1	0.6	0.4
Lu	0.1	0.1	0.0	0.1	0.1	0.1	0.1	0.1
ΣREE	55.0	30.4	33.9	55.9	28.4	142.7	56.2	68.8
ΣLREE/ ΣHREE	9.1	9.7	8.5	11.8	6.7	22.5	19.4	20.2
Ce/Ce* (N)	0.9	1.0	0.9	1.0	1.1	1.0	1.0	1.1
Eu/Eu* (N)	1.1	1.0	1.1	0.9	1.4	1.0	1.2	1.3

Data supplied by ACME Analytical Laboratories ltd. (Canada)

Table 5.6: contd.

Rock type	Mn-carbonate schist						Mn-calcite marble					
Sample	**DH114-A**	**DH116-A**	**DH116-B**	**DH140-A**	**DH140-C**	**DH140-D**	**DH114-K**	**DH114-C**	**DH114-E**	**DH116-H**	**DH116-J**	**DH114-O**
La	13.5	13.4	8.7	4.5	3.8	11.8	10.0	16.5	5.6	4.3	7.7	5.9
Ce	65.1	44.4	24.9	21.6	16.7	52.9	54.1	87.9	31.1	24.7	45.6	30.5
Pr	2.3	2.6	1.8	1.1	0.9	2.9	2.0	3.6	1.1	0.9	1.4	1.1
Nd	8.2	2.6	8.4	4.2	3.3	12.5	8.4	16.0	4.7	4.1	6.2	4.5
Sm	1.8	12.3	2.0	0.8	1.1	2.1	1.7	2.5	0.9	0.8	1.4	1.0
Eu	0.4	0.7	0.6	0.3	0.4	0.6	0.5	0.6	0.4	0.3	0.3	0.3
Gd	1.8	2.6	2.6	0.8	1.3	1.9	1.6	2.4	1.1	1.0	1.2	1.1
Tb	0.4	0.5	0.5	0.1	0.2	0.3	0.3	0.4	0.2	0.2	0.3	0.2
Dy	1.7	2.3	2.5	0.6	1.3	1.6	1.8	2.1	1.2	1.5	1.5	1.1
Ho	0.3	0.4	0.4	0.1	0.3	0.3	0.3	0.4	0.3	0.2	0.3	0.2
Er	0.9	1.2	1.4	0.4	0.8	0.9	0.9	1.2	0.8	0.6	1.0	0.5
Tm	0.1	0.2	0.2	0.1	0.1	0.1	0.1	0.2	0.1	0.1	0.1	0.1
Yb	0.9	1.4	1.3	0.4	0.7	0.8	1.0	1.1	0.5	0.7	0.8	0.5
Lu	0.1	0.2	0.2	0.1	0.1	0.1	0.1	0.2	0.1	0.1	0.1	0.1
ΣREE	97.5	84.6	55.3	34.8	31.0	88.7	82.6	135.0	48.0	39.5	67.8	47.1
ΣLREE/ ΣHREE	14.7	8.8	5.1	13.3	5.3	14.1	12.8	15.9	10.1	8.0	11.9	11.4
Ce/Ce* (N)	2.7	1.7	1.5	2.3	2.1	2.1	2.8	2.6	2.9	2.8	3.2	2.8
Eu/Eu* (N)	1.0	0.6	1.3	1.6	1.6	1.4	1.3	1.1	1.8	1.3	1.1	1.5

Data supplied by ACME Analytical Laboratories ltd. (Canada)

The lack of a significant positive Ce anomaly seems to suggest that Ce is present as the Ce^{3+} and did not become fractionated from the other REE. One sample in biotite schist (DH116-Q) displays a strong negative Eu anomaly while another shows a positive Eu anomaly in the graphite schist. This anomaly may be explained by enriched plagioclase in some samples. Otherwise, these random deviations are tentatively attributed to analytical errors.

5.3.1.2 Carbonate rocks

The samples of carbonate rocks show a ΣREE in the range 30 –140ppm. This is much lower and more variable than for the alumo-silicate rocks. But it is significantly elevated compared to data sets from other Mn-carbonate deposits. Mn-rich rocks of the Penganga Group, India, display ΣREE < 30ppm (Gutzmer and Beukes, 1998a) while those of the manganese ores in the Hotazel formation, Kalahari Manganese Field, South Africa are below 40ppm (Gutzmer and Beukes, 1998b).

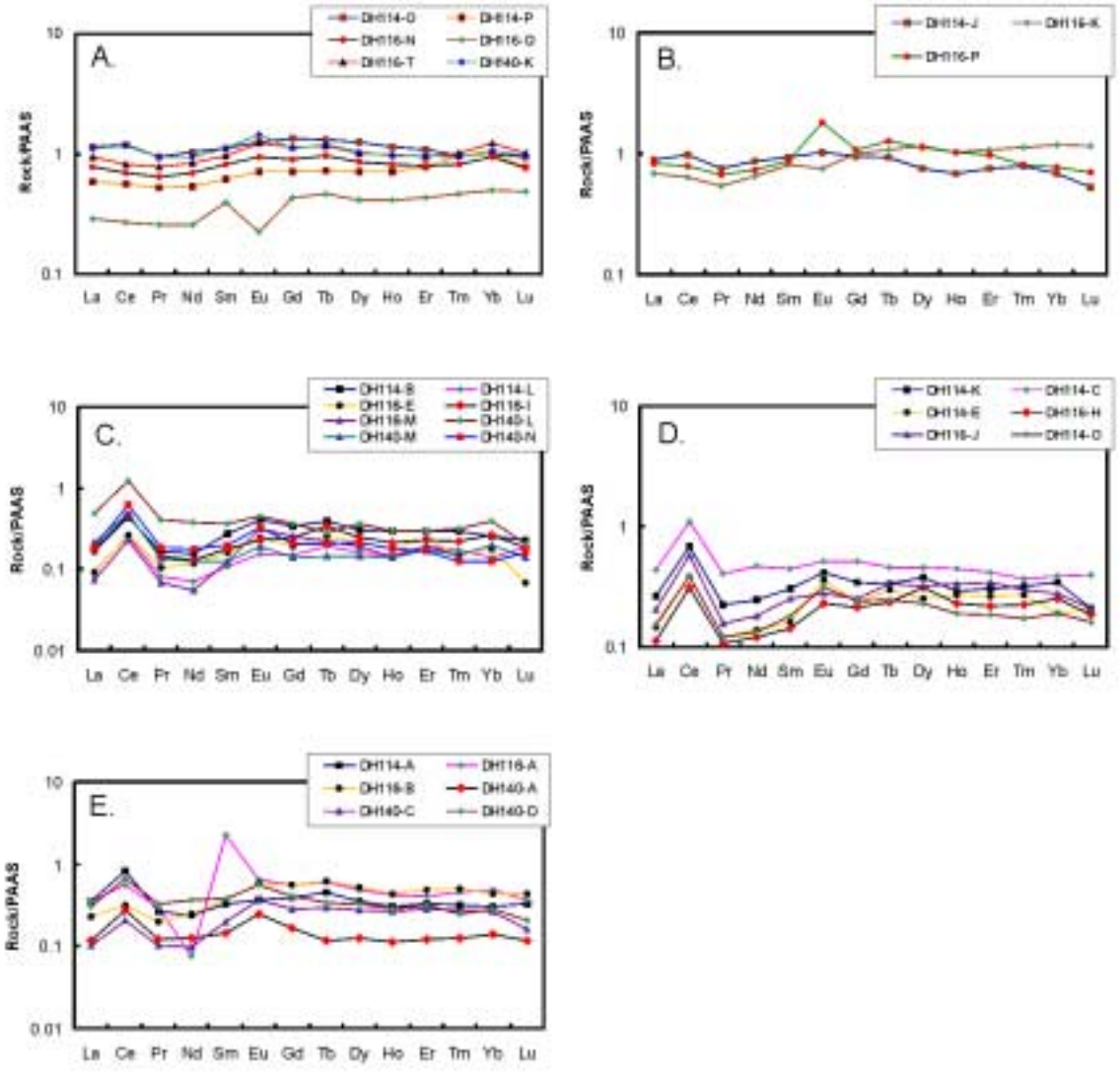

Fig.5.6: PAAS normalized REE patterns for whole rock analyses of the different lithological groups of the Serra do Navio deposit. A: Biotite schist; B: Graphite schist; C: Rhodochrosite marble; D: Mn-calcite marble; E: Mn-carbonate schist.

The covariation of ΣREE with Al_2O_3 for the carbonate rocks is only weakly positive (Fig. 5.5d). Normalized to PAAS, all the samples plot below the PAAS field (Fig 5.6). All three petrologic groups (rhodochrosite marble, Mn-calcite marble and Mn-carbonate schist) show positive Ce anomalies (0.9 – 1.1, 2.6 – 3.2 and 1.5 – 2.7, respectively). A strong covariation exists between the Ce anomaly and the MnO concentration (Fig.5.5g). Eu (Eu* in the range 0.6 – 1.8), on the other hand, has only a weak positive or no apparent anomaly. All samples are characterized by a very slight enrichment of LREE relative to the HREE. At least one sample (DH116-B) displays an unusual enrichment in Sm and depletion of Nd, a result tentatively attributed to an analytical artifact.

Systematic differences between the carbonate-rich lithologies and the alumo-silicate rocks are reflected in a rather flat REE distribution pattern for the alumo-silicates. This indicates that relative to the carbonate rock, REE incorporated into the alumo silicate rocks were less fractionated. In addition, ΣREE for carbonate rocks are much lower than for alumo-silicate rocks. The carbonate-rich lithologies display strong Ce positive anomalies, a feature absent in the alumo-silicates. Both groups, however, do show similar flat HREE patterns suggesting that most REE was introduced as part of the detrital clay mineral fraction.

5.2 Discussion

5.2.1 Alumo-silicate rocks

There is no systematic difference in major and trace element geochemistry between biotite schist and graphite schist. Systematic variations in major element geochemistry of the different samples of alumo-silicate rich rocks compared well to variations in the abundance of major mineral constituents. A mineral assemblage of plagioclase, quartz, and biotite in addition to spessartine porphyroblasts is typical. MnO appears to be hosted in spessartine only, while SiO_2, Al_2O_3, K_2O and Na_2O are incorporated into quartz, plagioclase and biotite. High Fe_2O_3 and MgO are attributed to the presence of chlorite.

A plot of trace elements on an Upper Continental Crust (UCC) spider diagram (Taylor and McLennan, 1981) shows a widely variable pattern with significant enrichment in Ba and depletions in K, Sr and P (Fig. 5. 4). This may suggest derivation from a differentiated felsic precursor. The similarity in distribution and concentration of trace elements such as Sc, Th, U, Zr, Nb and V shows that the processes controlling their distribution during and after sedimentation remained rather uniform. The strong positive correlations between Zr, Sc, TiO_2 and Al_2O_3 (Fig.5.5h) confirm that these elements are of detrital origin either as clay minerals or rock forming alumo-silicate minerals such as feldspars. The behavior of Ba is noteworthy. It covaries strongly with Al_2O_3, K_2O and Rb and weakly positive with MnO. It is thus suggested that the distribution of Ba is controlled by K-feldspar and not by plagioclase (Fig. 5.5b-c). The positive correlation between Sr and Ca may point to substitution of Sr for Ca in the lattice of plagioclase. Significant positive correlation between base metals (Co, Ni, Pb and Zn) and Fe_2O_3 can be explained by the observation that these elements are all concentrated in sulphide minerals (Fig.5.5f).

The high ΣREE, weak negative Eu anomaly and fairly flat REE distribution pattern all point to an ancient Upper Continental Crustal (UCC) provenance (McLennan et al., 1984). McLennan and Taylor (1991) report that post-Archean turbidites of Precambrian age show typical negative anomalies of Eu in the range 0.6 – 0.7 while anomalies (depletions or enrichments) are absent in the Archean. Turbidites from active margin settings with negative Eu anomalies are associated with more evolved (i.e. felsic) sources (McLennan and Taylor, 1991). The data set of alumo-silicate rocks at Serra do Navio is consistent with these conclusions. The alumo-silicates from Serra do Navio were possibly deposited as turbidites whose sediments were actually derived from evolved upper continental crust. The high ΣREE is consistent with the fact that clay minerals have a tendency to harbor significant amounts of REE.

5.2.2 Carbonate rocks

The major element geochemistry of this group of lithologies is characterized by predominance of MnO over SiO_2 and Mn/Fe ratios > 1. Within this group however, the

three lithological groups show salient differences. Rhodochrosite marble has the highest MnO content, LOI (corresponding to carbonate content), Mn/Fe ratios and lowest SiO_2 content. Mn-carbonate schist, in contrast, has lowest MnO, LOI, Mn/Fe and highest SiO_2 content amongst the three lithologies while Mn-calcite marble is intermediate in composition between the two lithological groups.

The separation of the three lithological groups with respect to SiO_2 concentration in particular, is clear and without overlap (Fig.5. 2). In rhodochrosite marble elevated MnO concentrations are attributed to abundance rhodochrosite only, while in Mn-calcite marble and Mn-carbonate schist they are attributed to the presence of both Mn-rich carbonates and Mn-silicates, in variable proportions. In samples that are marked by elevated SiO_2 concentrations, Mn is present as Mn-rich silicates (tephroite, rhodonite and spessartine).

SiO_2 is also present in many samples as recrystallized quartz or quartz infill of late fracture-hosted veinlets. Alumo-silicates such as spessartine, biotite and amphiboles could account for all Al_2O_3 but only a minor proportion of SiO_2. It is interesting to note that in contrast to SiO_2, Al_2O_3 is present only in very minor concentrations that are similar among the three lithological groups of carbonate rocks, and much lower than in alumo-silicate lithologies. Similarly, other constituents that are thought to reflect detrital influx (Zr, Ti, Cr) are low and uniform in concentration in the carbonate-rich rocks. Elevated and variable concentrations of SiO_2 are not correlated with these detrital components and it is thus assumed that SiO_2 in the carbonate-rich rocks does not represent a siliciclastic component, but more likely a chemically precipitated constituent, i.e. chert. Contents of typical carbonate constituents, MgO (2 – 8 wt. %) and CaO (4 – 11 wt. %), are elevated compared to the alumo-silicate lithologies and are positively correlated with MnO. Fe concentrations vary considerably but a distinct increase is observed with increasing SiO_2 concentration. This may suggest co-precipitation of SiO_2 and Fe_2O_3 and a separation of Fe and SiO_2 from Mn and CO_2 similar to that observed in intercalated BIF-MnF successions, notably in the Hotazel Formation in the Kalahari Manganese Field, South Africa (Beukes, 1983).

High Mn/Fe ratios suggest efficient fractionation of Mn from Fe during sedimentation. Separation of Mn from Fe is typically attributed to precipitation of Fe-sulphides (e.g. pyrite) in anoxic basinal black shales, whereas Mn becomes reduced, remobilized and reconcentrated under oxic conditions (Frakes and Bolton, 1992).

The trace element composition of the carbonate-rich lithologies shows some coherent characteristics but also some differences between the lithological groups. Relative to upper continental crust (UCC) trace element abundances are depleted in all samples. An important similarity between the three groups is the depletion of Rb, K_2O and Na_2O in all the samples, which is also reflected in the scarcity of alkali-bearing alumo-silicates. This conclusion is supported by the observation that alkali element concentrations are positively correlated with Zr, Al_2O_3 and TiO_2 concentrations (Fig. 5.5h), all constituents that are used to infer influx of siliclastic detritus. The weak correlation of Sr with CaO is assumed to indicate the local substitution of Sr in carbonate minerals.

Moderate to high Co, Ni and Zn show some correlation with Mn enrichment, suggesting that these elements are either co-precipitated or scavenged during Mn precipitation. Indeed modern marine Mn-oxyhydroxides crusts are known to be effective scavengers especially of Ni, Co and Cu (Elderfield et al., 1981). Studies on modern Mn nodules and crusts (e.g. Bonatti et al., 1972) generally differentiate Mn-rich sediments of hydrothermal or hydrogenous origin based on their major and trace element geochemistry. This is based on the fact that hydrothermal oxides are depleted in Co, Cu, Ni and Zn relative to hydrogenous deposits (Nicholson, 1992). Fig. 5.7 illustrates that Mn-carbonate rich rocks of the Serra do Navio deposit plot into the hydrothermal field of the triangular Mn-Fe-10x (Ni, Cu, Co) plot. However, this observation may just suggest that Mn-sediments precipitated rapidly and did not have sufficient time to concentrate base metals by scavenging.

The differences in slope in the covariation of V, Co, Ni and Zn with MnO (Figs. 5.5f) is used to invoke different host minerals for these elements in alumo-silicate and carbonate-rich rocks. The wide scatter of Ba concentrations, from being enriched to significant

depletion within the lithological groups is interesting. The Ba content in carbonate rich-rocks covaries weakly with K and Al_2O_3 but strongly positive with Mn (Fig.5.5b-c). This suggests that Ba was introduced with Mn, possibly as part of Ba-rich Mn-oxyhydroxide precipitate whereas in the alumo-silicate rocks Ba distribution is controlled by alkali feldspar.

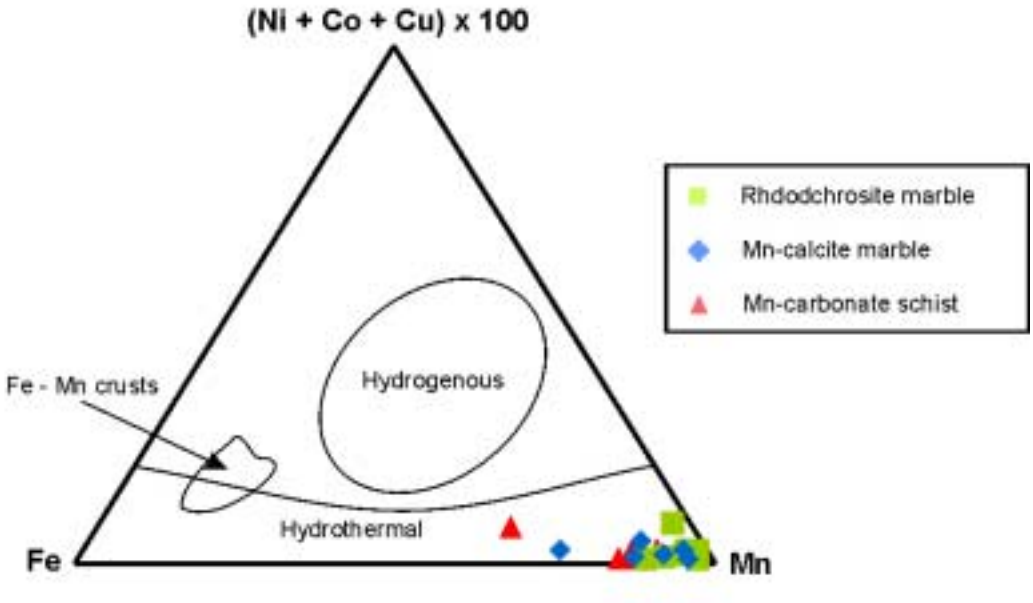

Fig. 5.7: Ternary diagram of (Ni + Co + Cu)*10 – Mn – Fe for the Mn-rich carbonate rocks of the Serra do Navio deposit. These occupy the Mn-rich corner of the hydrothermal field. Also shown are the fields for modern hydrogenetic and hydrothermal Fe – Mn crusts and nodules. Diagram after Bonatti et al. (1972).

The REE geochemistry for the carbonate-rich lithologies is rather similar. A major feature is the consistent and significant positive Ce anomaly and absence of any Eu anomaly. Studies on modern Mn nodules and Fe-Mn crusts show that there is a significant enrichment in Ce relative to other REE in these sediments (Elderfield and Greaves, 1981). This is also reflected in the positive covariation of MnO with Ce* (Fig.5.5g). This is very similar to the distribution of REE in modern marine hydrogenetic manganese crusts (Gutzmer and Beukes, 1998b). It can be used to confirm the sedimentary deposition of manganese as Mn-oxyhydroxides that were later diagenetically transformed into Mn-carbonates. This observation has been made for several other Mn-carbonate deposits (Gutzmer and Beukes, 1998b; Munteanu et al., 2004).

5.3 Summary

The alumo-silicate rocks are geochemically uniform, whereas the carbonate-rich rocks can be differentiated into three geochemically distinct groups that compare very well with petrological differences. Thus, only four lithological groups are presented in Fig .5.8.

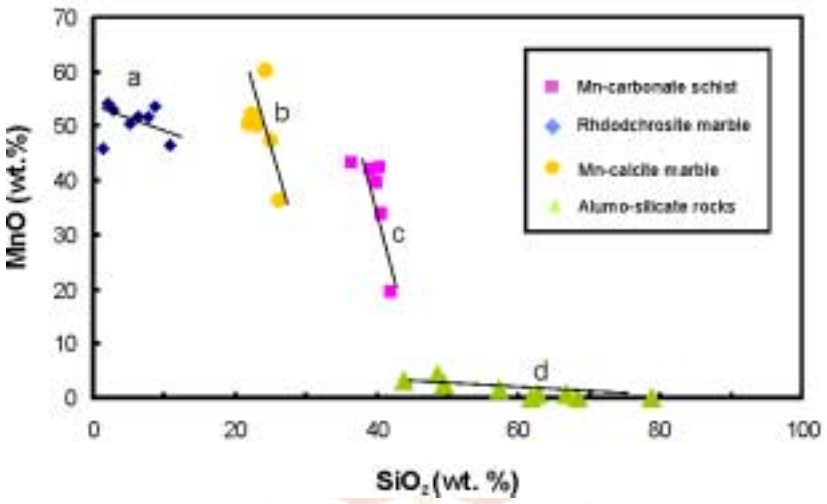

Fig.5.8: The binary MnO – SiO_2 plot reveals the presence of the four distinct geochemical groups in the sample set from the Serra do Navio deposit. (a): Rhodochrosite marble; (b): Mn-calcite marble; (c): Mn-carbonate schist; (d): Alumo-silicate rocks.

The slope for rhodochrosite marble is shallow while the slopes of Mn-calcite marble and Mn-carbonate schist are rather steep and similar (Fig 5.8). The shallow slope in rhodochrosite marble may suggest decoupling of Mn and SiO_2. The slope of the alumo-silicate rocks is nearly horizontal and indicates complete decoupling of Mn and SiO_2.

It is possible to illustrate the mixing of detrital fractions with a chemical fraction by studying suites of indicator elements. This has been previously done for iron formations using Fe/Ti and Al/(Al + Fe + Mn) ratios (Peter and Goodfellow, 1996). Al and Ti are taken to represent the detrital input while Fe and Mn represent the hydrothermal component. The use of this plot is here extended to the Mn-rich lithologies of the Serra do Navio deposit by replacing Fe/Ti with Mn/Ti (Fig.5.9). On the resultant plot Mn-carbonate rich rocks of the Serra do Navio are closely related to modern metalliferous

sediments (Mn crusts and nodules), but are well removed from modern pelagic sediments and modern terrigenous sediments field implying very little or no clastic input. There is also a clear overlap between the three Mn carbonate-rich lithological groups. However, the alumo-silicates plot in the fields defined by modern pelagic and terrigenous sediments. The distribution between the metalliferous sediments rocks and the siliclastics shows that there is only little mixing between alumo-silicate rocks and the carbonate-rich rocks with a clear gap between the two and that there is a clear distinction between sediments of chemical and clastic input (Fig 5.9).

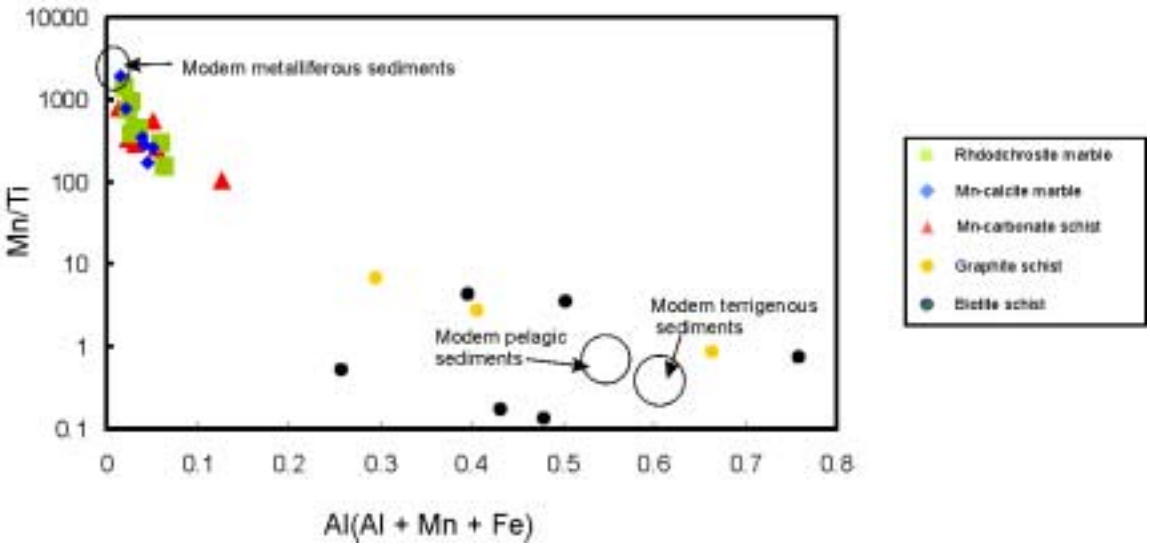

Fig.5.9: Diagram used to determine hydrothermal vs. detrital component based on Al/Ti and Fe-Mn content. After Peter and Goodfellow (1996)

The chemistry of marine and the freshwater oxides has been utilized to distinguish manganese deposits of different origins, i.e. supergene marine, shallow marine and freshwater environments (Nicholson, 1992). Diagnostic scatter plots have been proposed by Nicholson (1992) that clearly discriminate between different depositional environments.

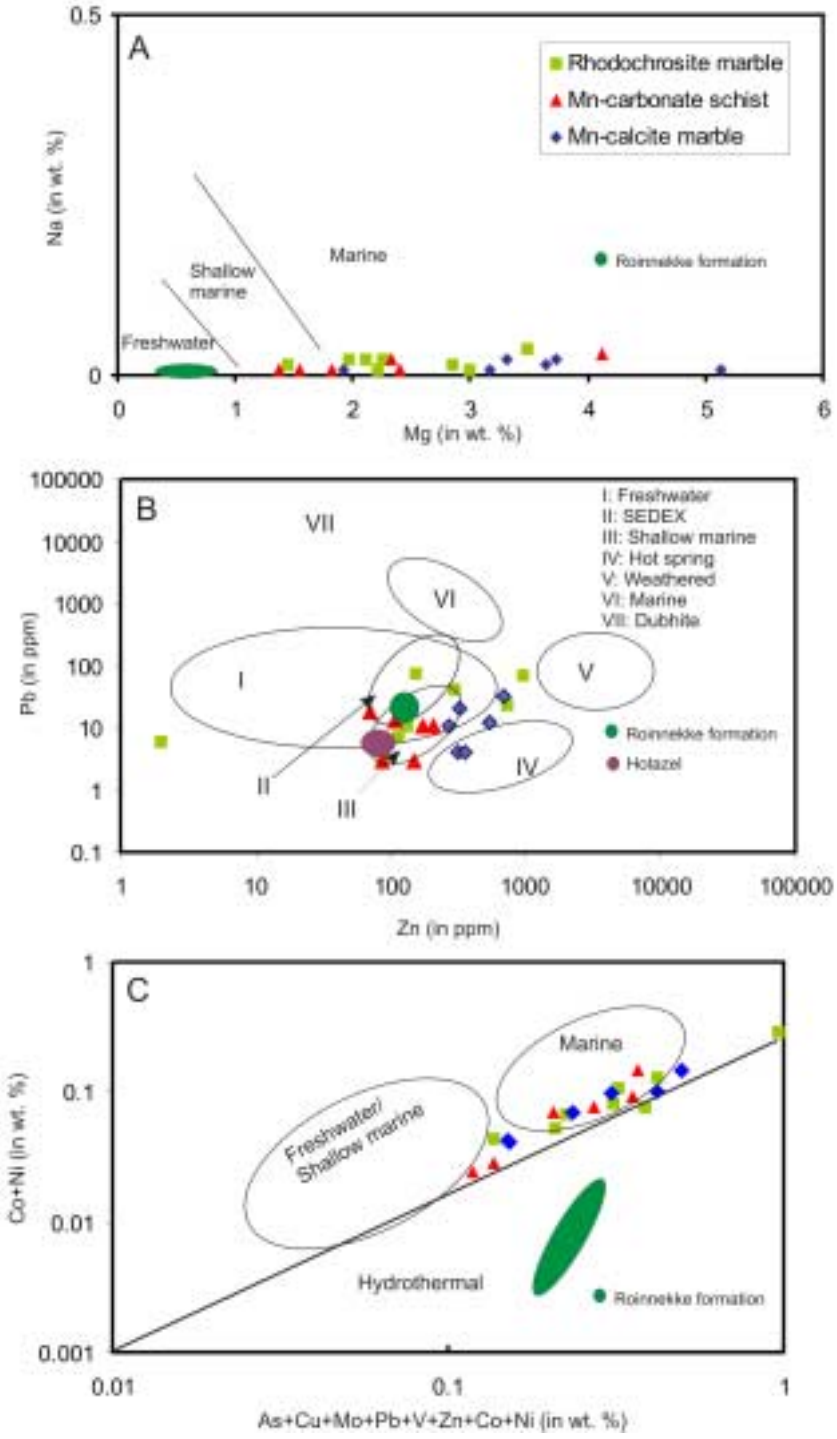

Fig. 5.10: Diagnostic plots to differentiate sedimentary manganese deposits from different depositional environments (after Nicholson, 1992). "Dubhite" = supergene Mn-oxyhydroxide accumulations formed at the expense of base metal mineralization (Nicholson, 1992). Rooinekke Formation data from Gutzmer and Beukes (1998) and Hotazel Formation data from Van Staden (2001).

These geochemical discrimination plots can be applied to the Mn carbonate-rich rocks of the Serra do Navio deposit. On an Mg vs. Na (wt.%) plot the shallow marine - marine (Fig. 5.10a) environment is favored. This is actually very coherent and in excellent agreement with the geochemistry of other sedimentary Mn-carbonate deposits (e.g. Nsuta, Ghana).

Similarly, on a Pb vs. Zn scatter diagram the carbonate rich rocks of the Serra do Navio plot in the freshwater – shallow marine field (Fig.10b). Also plotted are the fields occupied by the Mn-rich rocks of the Kalahari manganese field (Hotazel) and Mn-carbonates from the Paleoproterozoic Rooinkke formation (South Africa). On a binary diagram of Co + Ni (wt.%) vs. As + Co + Mo + Pb + V + Zn (wt. %) the Mn-carbonate-rich rocks of the Serra do Navio plot in the marine field (Fig.10c). All these plots suggest a marine or shallow marine environment of deposition for the Mn-carbonate rocks of the Serra do Navio deposit. The scatter is, however large and the results must be regarded as equivocal.

5.4 Stable Isotope Geochemistry

Stable carbon and oxygen isotope studies of carbonates are widely used to study geochemical processes in sedimentary geologic settings. The delineation of isotopic compositions yields both qualitative and quantitative constraints on modeling the properties of geochemical spheres during the geologic evolution of surface environments (Veizer et al., 1992).

Samples for stable isotope geochemistry were drawn from all three drill cores DH114, DH116 and DH140. Selection of samples was based on the abundance of carbonate mineral phases as determined by X-ray diffractometry. Rhodochrosite is the most abundant carbonate in most samples, often associated with other carbonates, such as Mn-calcite and/or kutnahorite. The latter constitutes the most abundant carbonate mineral in four samples. No effort was made to separate these carbonate minerals from one another

since the samples were submitted as aliquots of the same homogeneous sample powders of whole rock samples that were also submitted for major and trace element analyses.

Carbon and oxygen isotope compositions are respectively expressed in per mil, relative to PDB, a Cretaceous belemnite from the Pee Dee formation (Hoefs, 1980) as follows:

$$\delta\,^{13}C = \{(^{13}C\,/^{12}C)_{sample}/\,(^{13}C/^{12}C)_{PDB} - 1\} \times 1000$$

$$\delta\,^{18}O = \{(^{18}O/^{16}O)_{sample}/\,(^{18}O/^{16}O)_{PDB} - 1\} \times 1000$$

5.4.1 Results

Isotopic compositions of whole rock carbonates, together with dominant carbonate mineralogy investigated for the three drill cores are presented in Table 5.7. In drill core DH114 the $\delta^{13}C$ signature is consistent and quite uniform with a range between –7.9‰ and –6.6‰. An anomalous value of –9.4‰ is observed for the only kutnahorite-rich sample. A narrow range between –15.3‰ and –14.5‰ characterizes the $\delta\,^{18}O$ signature, while the only Mn-calcite dominated sample has an unusually depleted $\delta\,^{18}O$ of –17.1‰. In both cases it is deduced that the narrow variation is not a function of depth. It is however noted that signatures appear mineralogically controlled.

In drill cores DH116 and DH140 the scenario is similar, even though fewer samples were analyzed. In DH116 both $\delta\,^{13}C$ and $\delta\,^{18}O$ occupy narrow ranges between -6.3‰ and -4.3‰ and -15 ‰ to -14.4‰ respectively. DH140 is no different with constant $\delta^{13}C$ (-5.9 ‰) and $\delta\,^{18}O$ (average -14.8‰) values in excellent agreement with those observed in DH116.

5.4.2 Discussion

A plot of $\delta\,^{18}O$ vs. $\delta\,^{13}C$ (Fig. 5.11) reveals very little variation with respect to $\delta\,^{18}O$ values between all the samples from the three drill cores. Variations of $\delta\,^{13}C$, on the other hand, are marked, but appear to be controlled by the drill core from which the samples were taken. Mineralogy is a second important parameter that controls $\delta\,^{13}C$ variation.

Table 5.7: Stable isotope geochemistry and relative abundance of the carbonates in selected whole rock samples from drill core DH114, DH16 and DH140

Drill core	Mineral	Relative abundance of carbonates*	$\delta^{13}C$ PDB (‰)	$\delta^{18}O$ PDB (‰)
DH114-B	Rhod.	xxx	-6.8	-14.7
DH114-C	Mn-cal.	xxx	-7.7	-17.1
DH114-D	Rhod.	xxx	-7.1	-14.9
DH114-E	Kutn.	xxx	-7.9	-14.6
DH114-F	Rhod./Kutn	xxx/xx	-7.4	-14.8
DH114-G	Rhod./Kutn	xxx/x	-6.2	-14.4
DH114-I	Rhod.	xxx	-5.6	-14.5
DH114-K	Kutn.	xxx	-9.4	-15.3
DH114-L	Rhod.	xxx	-6.8	-14.6
DH116-C	Rhod./Kutn	xxx/x	-6.3	-14.4
DH116-D	Rhod./Kutn	xxx/x	-4.3	-15.0
DH116-E	Rhod.	xxx	-4.9	-14.5
DH140-M	Rhod.	xxx	-5.8	-14.8
DH140-N	Rhod./Kutn	xxx/xxx	-5.9	-14.8

* as determined by X-ray powder diffraction and petrographic studies NB: Rhod. = Rhodochrosite, Mn-cal. = Mn-calcite and Kutn = Kutnahorite. xxx = major (>50%), xx = minor (10 – 50%), x = trace (<10%).

There is a linear trend with wide variation for carbon and extremely narrow spread in oxygen (Fig. 5.11). Interestingly, variable $\delta^{13}C$ and consistent $\delta^{18}O$ values are observed in unmetamorphosed as well as metamorphosed Mn-carbonate sediments of variable ages (Fig. 5.12). There is excellent agreement with Mn-carbonate deposits of similar Paleoproterozoic age (2.3 – 2.1 Ga), most notably the Nsuta deposit (Ghana), but also the Kalahari manganese field (South Africa). This may indicate that Mn-carbonates in these deposits formed under similar conditions, possibly from ambient seawater. In agreement with Van Staden (2002), it is concluded that differences in isotopic composition reflect difference in the condition of formation of the Mn-carbonate rocks, and cannot be attributed to isotopic re-equilibration during metamorphism.

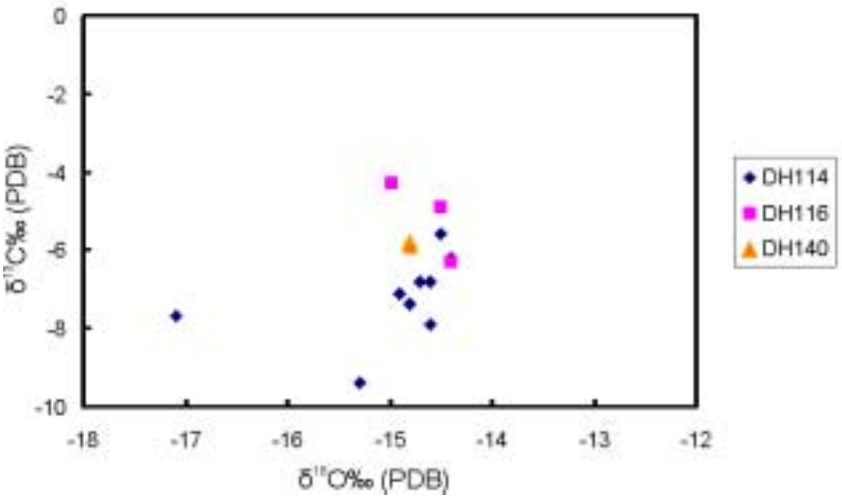

Fig. 5.11: Stable isotope composition ($\delta^{18}O$ vs. $\delta^{13}C$) of the Mn-carbonates at Serra do Navio deposit.

Different isotopic compositions almost certainly reflect differences in the sedimentary or early diagenetic environments in which the carbonates formed. Mn-carbonates in sedimentary host rocks are generally interpreted to have formed as a result of early diagenetic reduction of Mn-oxyhydroxides precipitates coupled with the oxidation of organic matter (Okita et al., 1988).

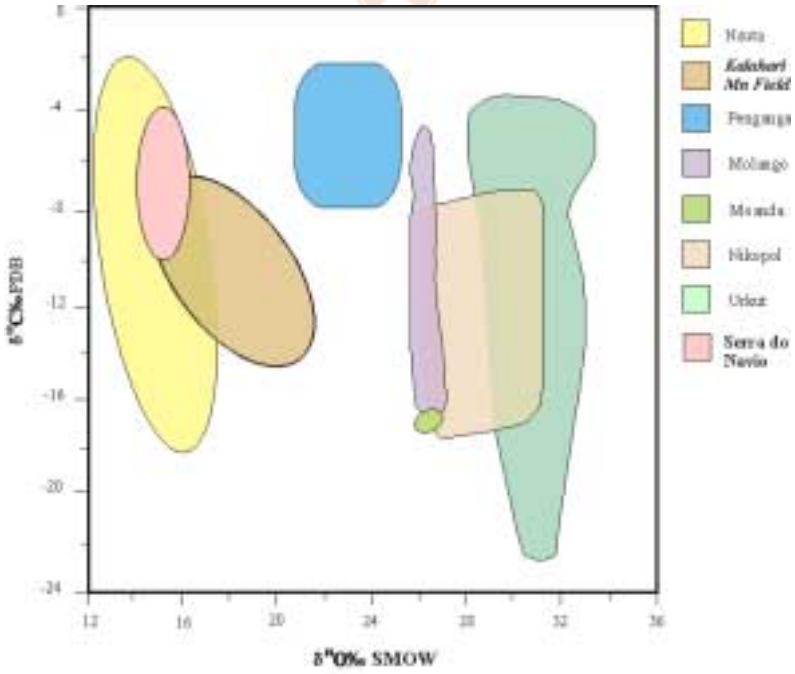

Fig. 5.12: Plot of $\delta^{18}O$ vs. $\delta^{13}C$ for the carbonate rocks at Serra do Navio In comparison to other manganese carbonate deposits.

Hence Mn-carbonates should have a $\delta^{13}C$ signature consisting of a mixture between inorganic CO_2 and organic carbon and a $\delta^{18}O$ determined by pore water oxygen derived from seawater. This seems to also hold true for the carbonates from the Serra do Navio deposit. On this basis then, the relatively light $\delta^{13}C$ composition of the carbonates at Serra do Navio may point to a diagenetic origin for the Mn-carbonates. Light $\delta\ ^{18}O$ values are attributed to low $\delta^{18}O$ present in seawater or diagenetic pore water. But the uniformity of the $\delta^{18}O$ isotopic ratios could also be used to suggest that the signature was homogenized by the interaction of the diagenetic carbonates with some post-diagenetic fluid, possibly before or during metamorphism. It could also just reflect uniform conditions of formation with respect to $\delta^{18}O$ composition of the pore water.